RSC Advances

ROYAL SOCIETY OF CHEMISTRY

www.rsc.org/advances

Mo_2C nanoparticles were successfully synthesized via a facile approach by hydrothermal carbonization method. Moreover, the effect of carburization agents of Ar, CH_4/H_2=0.2, and H_2 was investigated. Specially, the carburization behaviors and the evolution of Mo species in the samples during the carburization were extensively studied. The structures of catalysts experienced an extensive restructuring process during the carburization and in turn induced different performance in CO hydrogenation.

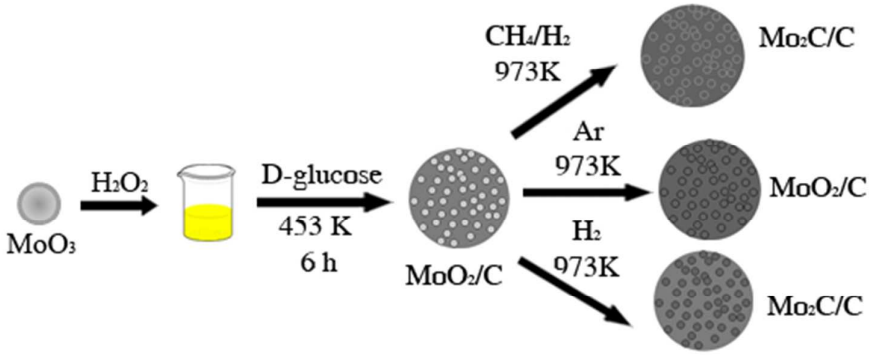

RSC Advances

RSCPublishing

PAPER

Preparation of nanostructured molybdenum carbides for CO hydrogenation

Cite this: DOI: 10.1039/x0xx00000x

Changcheng Liu,[a,b] Minggui Lin,[a] Kegong Fang,[a] Yan Meng[c] and Yuhan Sun[*c]

Received ooth January 2012,
Accepted ooth January 2012

DOI: 10.1039/x0xx00000x

www.rsc.org/

Novel Mo_2C/C nano/microcomposites were prepared via a facile approach by hydrothermal carbonization of a solution of glucose as a carbon precursor in the presence of ammonium heptamolybdate tetrahydrate. The samples were subsequently characterized by X-ray diffraction, X-ray photoelectron spectroscopy, thermal gravimetric analysis, N_2-physisorption, scanning electron microscopy and high-resolution transmission electron microscopy. The effect of carburization agents of Ar, CH_4/H_2=0.2, and H_2 was investigated. Specially, the carburization behaviours and the evolution of Mo species in the catalysts during the carburization and the effect on CO hydrogenation for higher alcohols synthesis were extensively studied. During the carburization, the catalyst structures experienced an extensive restructuring process and in turn induced the different performance in the higher alcohols synthesis. Moreover, the nanostructured molybdenum carbides synthesized by this method exhibited great performance in CO hydrogenation for higher alcohols synthesis.

1. Introduction

Molybdenum carbide has been extensively studied due to its unique physical and chemical properties including mechanical hardness, thermal stability, tolerant of carbon deposition and sulfur, and surface reactivity.[1-3] It has also been identified as a promising catalyst that can substitute noble metals in several heterogeneous reactions,[4-9] especially CO hydrogenation for higher alcohols.[10, 11]

So far, varies of methods have been investigated to synthesized β-Mo_2C nanoparticles, such as sonochemical method,[12] microwave-assisted method,[13] organic-inorganic hybrid method,[14] hydrothermal method,[15] and carbothermal hydrogenation reduction method.[16] Recently, the method of one-pot saccharides hydrothermal-carburization process to prepare metal-carbon materials has been extensively studied.[17-21] As the reducibility of saccharides, it is possible by this method to achieve the preparation of homogeneously dispersed metal nanoparticles within certain porous solid matrixes or permeable shells, where active nanoparticles are largely isolated and their agglomeration under reaction conditions can be prevented. The porous materials herein act as a physical barrier but still allow reactants and products traveling freely between bulk reaction media and catalyst surfaces.[19] Generally, the carbon-dispersed nanoparticles are prepared through direct carbonization of carbohydrates in the presence of metal species using hydrothermal process under mild conditions. Furthermore, this is an easy, economic and efficient strategy for the controllable preparation of nanostructured carbides, and can be large-scale manufacture and application.

Herein, we designed a one-pot hydrothermal cohydrolysis-carbonization process using glucose and ammonium molybdate as starting materials and successfully fabricated the carbonaceous spheres embedded with highly dispersed molybdenum carbide nanoparticles. The as-prepared materials were characterized by X-ray diffraction (XRD), X-ray photoelectron spectroscopy (XPS), N_2-physisorption, thermal gravimetric Analysis (TGA), scanning electron microscopy (SEM) and transmission electron microscopy (TEM). Based on these, the effect of carburization agent upon the catalytic properties was evaluated by CO hydrogenation.

2. Experimental

2.1 Synthesis

Commercially available solvents and reagents were used as received. Highly dispersed molybdenum carbide nanoparticles embedded with carbon were prepared via a facile hydrothermal method followed by carburization in a certain atmosphere. Typically, 2.88 g MoO_3 obtained from calcining $(NH_4)_6Mo_7O_{24}\cdot 4H_2O$ (AHM) was dissolved in 22 mL 30 wt.% aqueous H_2O_2 and 80 mL distilled water, followed by adding 19.82 g D-glucose (GL). Afterward, the solution was transferred to a Teflon-lined stainless steel autoclave (150 mL in volume) and hydrothermally treated at 453 K for 6 h. After cooling down, the dark product precipitate was filtrated, rinsed and dried. This as-synthesized sample was then loaded into a tube furnace and heated at 973 K for 4 h at a heating rate of 2 K/min in streams of Ar, 20 vol% CH_4/H_2, and H_2 (GHSV=6000 h^{-1}), respectively. Finally, the samples were quenched to ambient temperature and passivated with 2.0 vol% O_2/Ar (GHSV=1000 h^{-1}) before exposure to air. The carburized samples are denoted as Mo-Ar, Mo-CH, and Mo-H responding to treatment atmosphere of Ar, 20 vol% CH_4/H_2, and H_2. The sample before carburization is called Mo-Or.

2.2 Characterization

The bulk structure of the samples was measured by XRD (Rigaku D/max-RA, Cu Kα radiation, .λ = 1.542 Å). The dimension and morphology of the samples were determined using SEM (Hitachi High- Technologies Co. Ltd. 2.0 kV) and TEM (JEM-2010 FEF, 200kV). The specific surface area and pore volume of samples were detected using N_2 adsorption–desorption isotherms (Micromeritics ASAP-2000). Before analysis, the samples were degassed at 393 K for 12 h. The thermal behavior of samples was monitored using TGA (Setaram, Setsys Evolution, 16/18). During the experiment, the temperature was raised from room temperature to 973 K at a heating rate of 10 K/min in Ar, H_2 or 20 vol% CH_4/H_2, especially. Ar was used as a carrier gas with the flow rate nonuple to that of H_2 or 20 vol% CH_4/H_2. The content of carbon in samples was measured with a Carlo Erba 1106 EL Microanalyzer. Surface compositions of the samples were investigated with XPS (PHI-5300 X, Perkin-Elmer Physical Electronics Co.) using an Al Kα primary radiation. All binding energies were referenced to C1s of 284.6 eV.

2.3 CO hydrogenation for higher alcohols synthesis

1.0 mL sample (60-80 mesh) equivalently diluted with quartz granules were evaluated in a pressured fixed-bed reactor at 553K, 7.0 Mpa, 4000 h^{-1} with a H_2/CO ratio of 2:1 without any pretreatment. Effluents gases were analyzed using Carbosieve-packed column with TCD and Al_2O_3 column with flame ionization detector (FID). Propake-Q column with TCD and FID were applied to the analysis of water, methanol and other alcohol products in liquids.

3. Results and Discussion

3.1 Morphologies

In this method, highly dispersed molybdenum carbide nanoparticles embedded with carbon have been prepared in a large quantity with inexpensive ammonium molybdate and glucose as precursors. Fig. 1a gives the general morphology and structure of the sample prepared at 453 K for 6 h under hydrothermal conditions. As can be seen, the sample shows a porous structure comprised of small particles. After carbonization at 973 K for 4 h, there is nearly no difference in morphology of these samples, while more tiny particles appear on the surface, probably due to aggregation of Mo species and gasification of carbon at high temperature.

In order to investigate the microstructure features, the samples were further characterized by TEM. Shown in Fig. 2a,b, nanostructured molybdenum oxide embedded with carbon was readily formed after hydrothermal reaction but even prior to carburization treatment. The nanostructured molybdenum oxide particles were finely dispersed by carbon matrix. Additional, it could be clearly seen from Fig. 2a,b that the size of molybdenum oxide nanocrystals is of high degree of uniformity with about 4 nm (Table1). The lattice spacing of 0.34 nm and 0.24 nm could be assigned to the (-111) and (-211) plane of MoO_2 phase, which shall further confirmed by XRD analysis. After carburization, there is no significant change of the particle size of the encapsulated molybdenum species nanocrystals (Fig. 2c-h), elucidating the effectiveness of the carbon matrix in the Mo-Or to habit the crystal growth during the carburization treatment. The mean particle size of the Mo species synthesized under different carburization conditions are list in Table 1.

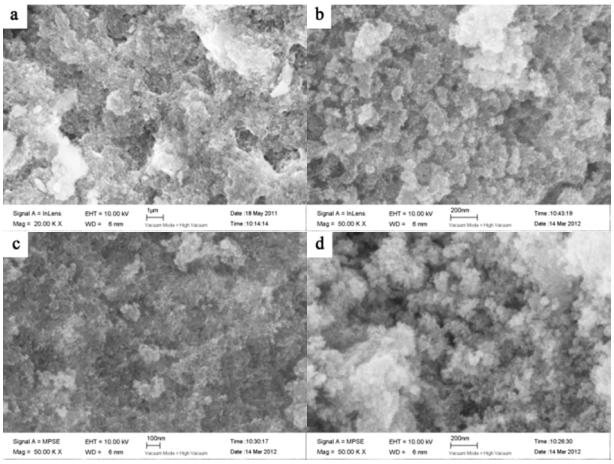

Fig. 1 SEM images of (a) Mo-Or, (b) Mo-Ar, (c) Mo-CH, and (d) Mo-H.

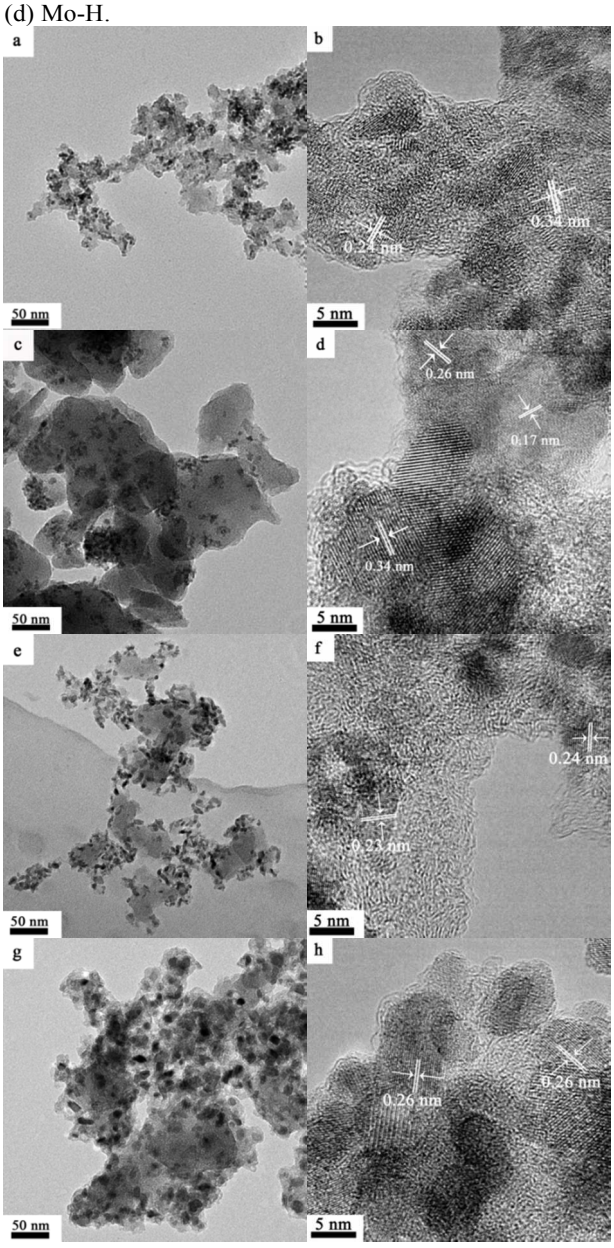

Fig. 2 TEM images of (a, b) Mo-Or, (c, d) Mo-Ar, (e, f) Mo-CH, and (g, h) Mo-H.

However, it could be seen that the mean particle size was still affected by the carburization agents, which is 5 nm for Mo-Ar, 6 nm for Mo-CH, and 11 nm for Mo-H. Moreover, the crystal phase of dispersed molybdenum oxide changed after carburization as expect, the lattice spacing of 0.23 nm, 0.17 nm and 0.26 nm could be assigned to (101), (100), and (102) plane of Mo_2C (Fig. 2d,f,h), as will be further discussed together with XRD analysis below (Fig. 3).

Besides, adventitious carbon is clearly observed in the figures and verified by the element content analysis (Table 1), which is the product obtained from hydrothermal carbonization of D-glucose.[22] Thus, it could be postulated that the unique combination of nano-sized Mo species particles and adventitious carbon might provide much more active sites than conventional molybdenum carbides. This approach is expected to offer an alternative opportunity for designing carbon supported nano-sized molybdenum carbide for CO hydrogenation due to some potential advantages of carbon support.[23]

3.2 Phase and textural structure

The crystallographic structure of the samples was characterized by XRD. From XRD pattern of Mo-Or (Fig. 3a), the poorly crystalline phase is assigned to MoO_2 (2θ=26.2°, 37.0°, 41.2°, 53.0°, 53.5°, 60.2° and 66.6°, JCPDS No. 32-0671), agreed with the HRTEM in Fig. 2b. No additional peaks are found, confirming that the composite material corresponds to MoO_2 embedded by carbon. Additional, the carbonaceous phase in these samples is amorphous, since no graphtic carbon peaks observed. After carburized in Ar atmosphere, the major diffraction peaks of Mo-Ar are still assigned to MoO_2. The peaks assigned to the peaks of β-Mo_2C (JCPDS No. 35-0787) crystalline phase are poor, indicating that not much MoO_2 carbidized to β-Mo_2C in the Ar on the conditions of 973 K for 4 h. These results are confirmed by HRTEM in Fig. 2d, the most of lattice spacing is of 0.34 nm belonging to MoO_2. As for the sample of MoC-H, the crystallinity of β-Mo_2C phase is significantly improved with major diffraction peaks such as 2θ=34.4°, 38.0°, 39.4°, 52.1°, 61.5°, 69.6°, and 74.6° appeared and enhanced. In addition, the peak assigned to MoO_2 is too poor to be observed, verified by Fig. 3c. While for the sample of Mo-CH (Fig. 3d), the poorly crystalline peaks could not be distinguished, even no peaks assigned to MoO_2, indicating that MoO_2 in Mo-Or changed after carbonization in 20 vol.% CH_4/H_2. Nevertheless, in Fig.2f the lattice spacing of 0.24 nm and 0.23 nm could be assigned to (-211) plane of MoO_2 and (101) plane of Mo_2C. Therefore, these peaks could be assigned to β-Mo_2C, though not all MoO_2 transformed to Mo_2C under the conditions. Above all, it could be concluded that different atmospheres led to different carburization and crystallinity degrees of molybdenum carbide. Referred to the work of Z.-Q. Wang[4] and H.-M. Wang[24], these results could be explained by the fact that the higher reactivity of H_2 benefits the reduction of MoO_2 and the formation of β-Mo_2C at lower temperature.

The N_2 adsorption–desorption isotherms for the samples are displayed in Fig. 4. The isotherms of all samples are of type IV with the hysteresis loops at relative pressure in the range of 0.4-1.0, confirming the mesoporous network. The corresponding pore size distribution calculated using BJH method[25] are shown in Fig. 5. These curves displayed different pore distribution center for every sample. For Mo-Or, two peaks centered at 15.1 nm and 32.2 nm appear. After carburization, the overall pore distribution center trends smaller. For Mo-CH, the pore distribution is centered at 11.3 nm, while for Mo-Ar, two peaks centered at 3.1 nm and 15.4 nm appear, and for sample of Mo-H, the peak centers at about 6.9 nm. That probably resulted in the different carbon left in the samples that provided the porosity.

The BET surface area (A_{BET}), total pore volume (TPV) and average pore diameter (d) of samples are presented in Table 1. The sample of Mo-Or obtained from hydrothermal treatment is porous, and the BET surface area is 38.8 m^2g^{-1}. After carburization, the BET surface area obviously increased except for Mo-H. As tabulated in Table 1, Mo-H showed the lowest surface area (A_{BET}=20.6 m^2g^{-1}) and the smallest total pore volume (TPV=0.06 cm^3g^{-1}) compared to others. Mo-Ar showed the largest surface area (A_{BET} =305.6 m^2 g^{-1}) and biggest total pore volume (TPV=0.48 cm^3g^{-1}), while for Mo-CH, the surface area is 153.2 m^2g^{-1}, and total pore volume is 0.36 cm^3g^{-1}. Combined with element analysis and TEM images, the

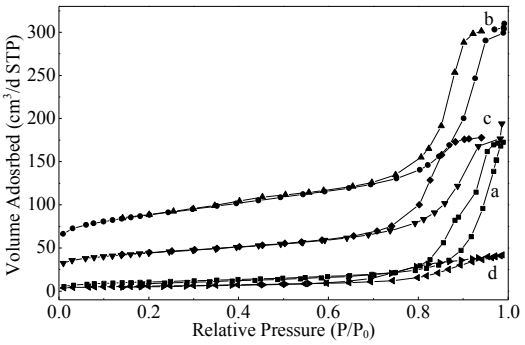

Fig. 4 N_2 adsorption-desorption isotherms (at 77K) of (a) Mo-Or, (b) Mo-Ar, (c) Mo-CH, and (d) Mo-H.

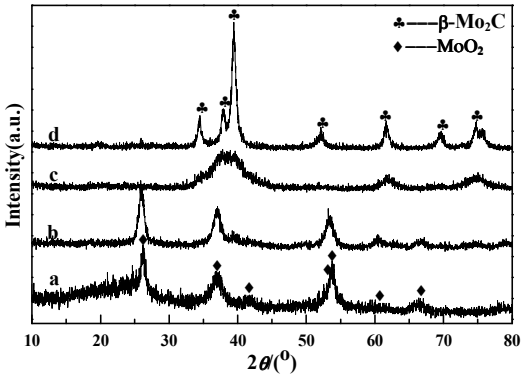

Fig. 3 XRD patterns of (a) Mo-Or, (b) Mo-Ar, (c) Mo-CH, and (d) Mo-H.

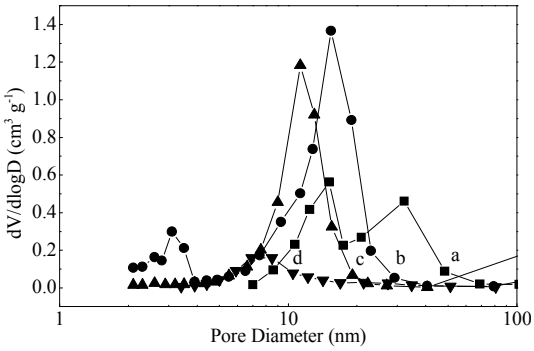

Fig. 5 The pore size distribution patterns of (a) Mo-Or, (b) Mo-Ar, (c) Mo-CH, (d) Mo-H.

Table 1. Textural parameters of the samples

Sample	Carbon content[1] (wt.%)	Surface atom content[2] (mol.%)			A_{BET} (m^2g^{-1})	TPV (cm^3g^{-1})	d (nm)	Dc[3] (nm)	Di[4]
		C	Mo	O					
Mo-Or	42.73	68.84	2.39	28.77	38.8	0.27	25.9	<4	4
Mo-Ar	39.80	80.75	4.59	14.66	305.6	0.48	6.28	<4	5
Mo-CH	35.02	78.55	10.25	11.20	153.2	0.36	12.54	<4	6
Mo-H	5.28	48.78	19.06	32.16	20.6	0.06	9.33	8	11

[1] Measured with Carlo Erba 1106 EL Microanalzer.
[2] Calculated from XPS data (Mo_{3d}, C_{1s} and O_{1s}).
[3] Crystalline size, obtained by Scherrer equation: Dc=0.89λ/ (β cos θ).
[4] Mean particle size, observed from HRTEM.
A_{BET} — BET surface area, T_{PV} — Total pore volume, d—Average pore diameter.

differences of texture can be derived from the carbon materials in the network of samples.

To have a better understanding on the carbonization process, thermogravimetric analysis was further employed in this study. As shown in Fig. 6, the weight loss below 450 K is generally attributed to evaporation of adsorbed water in all the cases.[19] When the sample of Mo-Or carburized in H_2 or CH_4/H_2, The TG curve exhibited the main weight loss between 450 and 1000 K, which could be attributed to the decomposition of the carbonaceous materials and the reduction-carburization of molybdenum oxide. The decomposition of carbonaceous materials would results in generating the porosity, ensuring better accessibility of the encapsulated molybdenum carbide to the reaction.[19] H_2 would prefer to lead carbon-source of precursors to flee in the carburization progress, evidenced by the fact that more brown tarry substance present at the end of quartz tube after carburization process. Additional, CH_4 could act as carbon-donator at higher temperature for the sample

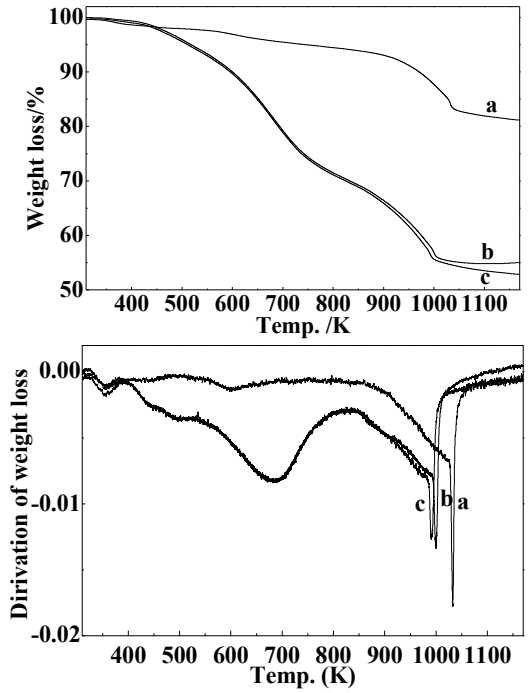

Fig. 6 The TGA and DTG curves of (a) MoC-Ar, (b) MoC-CH_4, and (c) MoC-H.

carburized in CH_4/H_2,[26] verified by the carbon content in the samples. On the other hand, the weight loss at the range of 600-700 K would be ascribed to the reduction of MoO_3 to MoO_2, the presence of MoO_3 could be from the oxidation of MoO_2 and Mo_2C, though no peaks assigned to MoO_3 for the samples of Mo-H and Mo-CH in the XRD (Fig. 3). Moreover, the peaks at about 1000 K could be considered as the carburization of MoO_2 to Mo_2C. As for the TGA of pure Ar, the curve exhibited a gradual and not pronounced weight loss in the range of 450 and 1000 K, which could be attributed to the partial elimination of organic volatiles from the carbonaceous matrix and the transformation of MoO_3 to MoO_2. For Ar the obvious weight-loss appeared at about 1050 K, much higher than the others. The different temperature of the samples at which the carburization occurred implied that the presence of H_2 apparently decreases the reduction temperature, well consistent with the XRD results and others.

3.3 Surface chemistry

The XPS measurement was conducted to investigate the surface chemistry of the carburized samples. The Mo3d and C1s spectra with fitting curves spectra are illustrated in Fig. 7, the surface compositions calculated from XPS spectra for all the samples are shown in Table 1 and the quantitative analysis of Mo3d signals for synthesized samples are shown in Table 2. In Fig. 7, three peaks located at 226.0, 228.9, and 232.5 eV in Mo3d spectra are observed for the samples except Mo-Or. For the sample of Mo-Or, the major molybdenum species on its surface are Mo^{6+} ($3d_{5/2}$=234.6 eV) and Mo^{6+}-Mo^{5+} ($3d_{5/2}$=232.4 eV), yet the content of Mo^{5+}-Mo^{4+} ($3d_{5/2}$=230.8 eV) is little. However, our XRD results reveal only MoO_2 phase in the sample (Fig. 3a), the conflict could be explained that the surface of the hydrothermally synthesized MoO_2 nanocrystals with low crystallinity was easily to be oxidized to higher states during the XPS sample preparation and handling.[19,27] After carburization, the overall peaks of Mo3d spectra turn to lower states and the molybdenum species with low oxidation states become more and observable, that is coincide with XRD analysis. For the sample of Mo-Ar, the major molybdenum species, Mo^{6+} ($3d_{5/2}$=233.1 eV), Mo^{5+} ($3d_{5/2}$=231.8 eV) and Mo^{4+} ($3d_{5/2}$=229.9 eV), are found on its surface. However, there is no peak belonged to carbidic molybdenum observed, although our XRD and HRTEM results reveal poorly crystallized β-Mo_2C phase in this sample (Fig. 3a, 2d). It could be attributed to the ambient oxidation which turns surface β-Mo_2C nanocrystals to molybdenum oxides.[19,27] For the sample of Mo-CH, the molybdenum species with lower oxidation states, Mo_2C ($3d_{5/2}$=228.6 eV) and MoO_2 ($3d_{5/2}$=229.5 eV), become more and observable (Table 2), which could be attributed to the carburization in CH_4/H_2 improved crystallinity. Nonetheless, the XRD analysis reveals only poorly crystallized β-Mo_2C are detected in the sample. Again, the Mo^{6+} ($3d_{5/2}$=233.0 eV) and

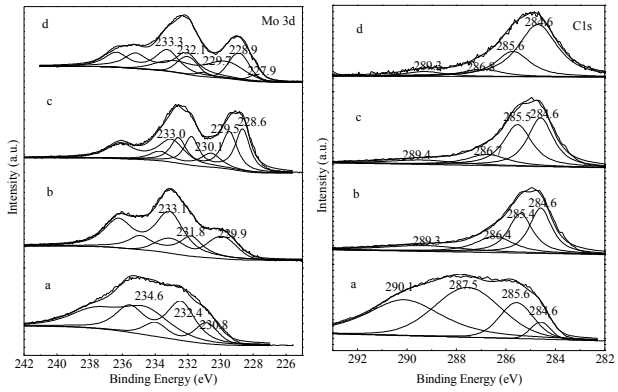

Fig. 7 Mo3d and C1s XPS spectra of (a) Mo-Ar, (b) Mo-CH,(c) Mo-H.

Mo^{5+}-Mo^{4+}components ($3d_{5/2}$=230.6 eV) observed herein could be attributed similarly to the ambient oxidation which turns surface MoO_2 and β-Mo_2C nanocrystals to α-MoO_3 and H_xMoO_3 surface species.[19,27] While, for the sample of Mo-H, the oxidation states of molybdenum species are further lower than the others, even Mo^0 ($3d_{5/2}$=227.9 eV) appeared in the sample. Clearly, higher reduction degree of Mo species in the sample of Mo-H is achieved.

The Cls spectrum shows the presence of four overlapping XPS peaks. For Mo-Or, the major peaks at 287.5 and 290.1 eV are attributed to surface carbonyl or quinone groups (>C=O) and carboxylic groups, esters, or lactones (-COO-), probably due to the carbon materials produced from glucose.[28-30] After carburization, these peaks with higher BEs significantly decreased, and the major peak is at 284.6 eV assigned to the surface C-C bond belonging to amorphous carbon as reported by several authors.[28-30] The other peaks located at aroud 285.5 and 286.7 eV are attributed to hydroxyl groups or ethers (C-OH) and C-O-C, respectively. The signal for the carbon atoms in the carbide form is very weak and almost cannot be distinguished clearly, even though in Mo3d spectrum the peak belonged to carbidic molybdenum observed. The surface compositions

Table 2 Quantitative analysis of Mo3d signals for synthesized samples

Sample	Assignment	B.E./eV	Area/%
Mo-Or	Mo^{6+}	234.6	43.7
	Mo^{6+}-Mo^{5+}	232.4	40.3
	Mo^{5+}-Mo^{4+}	230.8	16.0
Mo-Ar	Mo^{6+}	233.1	53.7
	Mo^{5+}	231.8	23.5
	Mo^{4+}	229.9	22.8
Mo-CH	Mo^{6+}	233.0	28.2
	Mo^{5+}-Mo^{4+}	230.6	13.6
	Mo^{4+}	229.5	28.4
	Mo^{2+}	228.6	29.8
Mo-H	Mo^{6+}	233.3	24.6
	Mo^{5+}	232.1	27.2
	Mo^{4+}	229.7	23.5
	Mo^{2+}	228.9	20.6
	Mo^0	227.9	4.1

calculated from XPS spectra are shown in Table 1, it could be expected that various amount of carbon on the surface will result in different catalytic performance in CO hydrogenation.

4. Catalytic performance

Finally, to test the catalytic properties of nanostructured β-Mo_2C, a preliminary study on CO hydrogenation reaction for higher alcohols synthesis using the as-prepared materials was carried out. As comparison, the β-Mo_2C of bulky counterpart obtained by TPRe method (marked as MoC-TPRe) was also applied to the reaction.[31,32] The detailed reaction results are summarized in Table 3 and 4. Generally, the performance of nanostructured molybdenum carbides synthesized by this hydrothermal carburization method is better than that of the Mo_2C obtained by TPRe method in the reaction. Moreover, the carburization gases led these catalysts with different structural and surficial properties, and then specifically manifested in the performance of CO hydrogenation. As shown in Table 3, the CO conversion of the catalysts varied in a wide range, for MoC-Ar is only 12.19 C%, while that is 92.06 C% for MoC-H, 66.55 C% for MoC-CH_4, and 55.79 C% for MoC-TPRe. As can be appreciated, transition metal carbides have been shown to possess better CO hydrogenation activity than the corresponding oxides, and the higher level of carburization, the higher activity of catalyst.[1] Furthermore, the activity is closely related to the Mo species with lower valence of the surface of catalysts.[1,33,34] Moreover, the XPS analysis results (Fig. 7 and Table 2) show that the amount of that is followed the sequence: MoC-H > MoC-CH_4 > MoC-Ar. Combined with the XRD patterns (Fig. 3), it could be concluded that the activity in CO conversion is well in accordance with the degree of carburization. Additional, the textural properties of these materials could also play a role, and the highly porous of carbon materials would enable reactants to reach the active molybdenum species nanocrystals. Then, the higher CO conversion of MoC-H and MoC-CH_4 than MoC-TPRe would be ascribed to the mesoporous structure and high surface area of the synthesized nanostructured catalysts, as the MoC-TPRe synthesized here is nonporous and the BET surface area is only 5 m^2g^{-1}. Compared with Mo-CH, the lesser carbon in the sample of Mo-H would favor more molybdenum species to react in the reaction and show higher activity. On the other hand, the selectivities towards the products exhibit different trends. It is known that the formation of alcohols is related to the surface stoichiometry and to the extent of carburization, whenever the level of carburization is too high, even only hydrocarbons are formed.[1] Combined with XRD, it is clearly seen that the trend of selectivity towards alcohols reverses with the degree of carburization of the samples. As seen in Table 3,

Table 3 The performance of catalysts in CO hydrogenation[1]

Cat.	CO Conversion (C%)	Yield (g/ml/h)		Selectivity[2] (wt.%)	
		Alcohols	Hydrocarbon	ROH	CHn
Mo-Ar	12.19	0.026	0.069	27.06	72.94
Mo-CH	66.55	0.038	0.405	8.67	91.33
Mo-H	92.06	0.026	0.676	3.71	96.29
MoC-TPRe	55.79	0.004	0.331	1.12	98.88

[1] Reaction conditions: H_2/CO=2.0, T=553 K, P=7.0 MPa, GHSV=4000 h^{-1}.
[2] Calculated on a CO_2 free basis.

Table 4 Alcohols and hydrocarbon distributions over the catalysts[1]

Cat.	Alcohol distribution (wt.%)					Hydrocarbon distribution (wt.%)				
	MeOH	EtOH	PrOH	BuOH	C_5^+OH	CH_4	C_2H_6	C_3H_8	C_4H_{10}	C_5^+H
Mo-Ar	72.24	20.34	6.10	1.32	0.00	47.17	25.84	16.28	6.08	4.63
Mo-CH	72.58	17.43	7.89	1.99	0.12	50.36	25.73	15.20	5.48	3.23
Mo-H	87.04	7.65	3.28	1.14	0.88	41.52	27.75	17.72	6.38	6.63
MoC-TPRe	83.89	10.51	4.06	1.54	0.00	49.74	23.19	15.87	6.04	5.16

[1] Reaction conditions: $H_2/CO=2.0$, T=553 K, P=7.0 MPa, GHSV=4000 h^{-1}.

the nanostructured catalysts give better selectivity towards alcohols, meaning the advantage of this method. As can be appreciated, Mo-Ar gives the highest selectivity towards alcohols (27.1%) though it performs the lowest activity. Moreover, in the absence of MoC-TPRe, Mo-H shows the lowest selectivity towards alcohols (only 3.7%) even it has the highest activity. As shown in Table 3 and 4, it can be seen that the major products over these catalysts are C_1–C_4 hydrocarbons, the yield of alcohols in the products is much lower than hydrocarbons for all the catalysts, and methanol is the main one in alcohol products, that is particular characteristic of β-Mo_2C in CO hydrogenation.[11] Combined with XRD results, it could also be seen that the trend of produce of methanol parallels with the carburization degree of catalysts, but the trend of methane reversed with that. As for Mo_2C, it is proposed to be a dual-site catalyst involving two types of molybdenum species,[34] namely the low valence molybdenum (Mo^I, I=0-2) and the high valence molybdenum (Mo^{II}, II = 4-5) species. The Mo^I species is the site for CO dissociation, hydrogenation and chain propagation to form surface alkyl species, while the Mo^{II} species is the site for molecularly adsorbed CO insertion and alcohol formation.[32] Together with XPS and XRD, it could be noticed that the more Mo^I species and less Mo^{II} of the Mo-H with higher carburization degree favor the chain propagation of hydrocarbons and suppress the chain propagation of alcohols, leading to more methanol and less methane in the catalyst. Therefore, to realize a desired Mo_2C catalyst for higher alcohol synthesis, it is necessary to precise control the carburization progress.

5. Conclusions

High dispersed β-Mo_2C nanoparticles have been successfully synthesized by a facilely hydrothermal method followed by a temperature-programmed carburization progress under different atmospheres. The subnanometer contact between molybdenum oxides and D-glucose molecules in the hydrothermal treatment remarkably facilitates the achievement of Mo_2C nanoparticles with large surface and enriched meso-porosity, which benefits the good performance in the production of alcohols from CO hydrogenation. In addition, various atmospheres led to different degree of carburization and matrix morphology under the same conditions, the sample carburized in Ar appeared only surficial carburized, but the surface-bulk of sample carburized in H_2 is homogenous. All the difference of structure and surface is revealed by the performance of CO hydrogenation.

Acknowledgements

The authors acknowledge the financial support from the State Key Foundation Program for Development and Research of China (Contract No. 2005CB221402), the National High Technology Research and Development Program of China (Nos. 2012AA051002), the Strategic Priority Research Program of the Chinese Academy of Sciences (Nos. XDA01020304), and the projects of National Natural Science Foundation of China (Nos. 21103217).

Notes and references

[a]State Key Laboratory of Coal Conversion, Institute of Coal Chemistry, Chinese Academy of Sciences, Taiyuan 030001, Shanxi, P.R. China
[b]University of Chinese Academy of Sciences, Beijing, 100049, P.R. China
[c] Low Carbon Conversion Center, Shanghai Advanced Research Institute, Chinese Academy of Sciences, Shanghai, 201203, P.R. China

Electronic Supplementary Information (ESI) available: See DOI: 10.1039/b000000x/

1. Leclercq L, Almazouari A, Dufour M, Leclercq G, in The Chemistry of Transition Metal Carbides and Nitrides, ed. Oyama ST. Glasgow, Blackie, 1996, pp. 345-361.
2. S. A. JANSEN and R. HOFFMANN, *Surf. Sci.*, 1988, **197**, 474.
3. H. H. Hwu and J. G. Chen, *Chem. Rev.*, 2005, **105**, 185.
4. Z.-Q. Wang, Z.-B. Zhang and M.-H. Zhang, *Dalton Trans.*, 2011, **40**, 1098.
5. A. Szymanska-Kolasa, M. Lewandowski, C. Sayag, D. Brodzki and G. Djéga-Mariadassoub, *Catal. Today*, 2007, **119**, 35.
6. J. Han, J. Duan, P. Chen, H. Lou, X. Zheng and H. Hong, *Green Chem.*, 2011, **13**, 2561.
7. M. Zheng, Y. Shu, J. Sun and T. Zhang, *Catal. Lett.*, 2007, **121**, 90.
8. A.R.S. Darujati, and W. J. Thomson, *Appl. Catal A*, 2005, **296**, 139.
9. S. Liu, L. Wang, R. Ohnishi and M. Lchikawa, *Kinet. Catal.*, 2000, **41**, 132.
10. H. C. Woo, K. Y. Park, Y. G. Kim, I.-S. Nam, J. S. Chung and J. S. Lee, *Appl. Catal.*, 1991, **75**, 267.
11. S. Zaman and K. J. Smith, *Catal. Rev.*, 2012, **54**, 41.
12. N. A. Dhas and A. Gedanken, *Chem. Mater.*, 1997, **9**, 3144.
13. M. Pang, C. Li, L. Ding, J. Zhang, D. Su, W. Li and C. Liang, *Ind. Eng. Chem. Res.*, 2010, **49**, 4169.
14. Q. Gao, C. Zhang, S. Xie, W. Hua, Y. Zhang, N. Ren, H. Xu and Y. Tang, *Chem. Mater.*, 2009, **21**, 5560.
15. B. Sun, L. Xu, K. Tang, L. Wang, Z. Ju and Y. Qian, *Cryst. Res. Technol.*, 2012, **47**, 467.
16. X. Li, D. Ma, L. Chen and X. Bao, *Catal. Lett.*, 2007, **116**, 63.
17. G. Yu, B. Sun, Y. Pei, S. Xie, S. Yan, M. Qiao and K. Fan, *J. Am. Chem. Soc.,* 2010, **132**, 935.
18. L. She, J. Li, Y. Wan, X. Yao, B. Tu and D. Zhao, *J. Mater. Chem.*, 2011, **21**, 795.
19. J. Dou and H. C. Zeng, *J. Phys. Chem. C,* 2012, **116**, 7767.
20. C. Avendano, A. Briceno, F. J. Mendez, J. L. Brito, G. Gonzalez, E. Canizales, R. Atencio and P. Dieudonne, *Dalton Trans.*, 2013, **42**, 2822
21. W. Wang, G. Ding, T. Jiang, P. Zhang, T. Wu and B. Han, *Green Chem.*, 2013, **15**, 1150.

22. M. Sevilla and A. B. Fuertes, *Chem.-Euro. J.*, 2009, **15**, 4195.
23. X. Li, L. Feng, Z. Liu, B. Zhong, D. B. Dadyburjor and E. L. Kugler, *Ind. Eng. Chem. Res.*, 1998, **37**, 3853.
24. H.-M. Wang, X.-H. Wang, M.-H. Zhang, X.-Y. Du, W. Li and K.-Y. Tao, *Chem. Mater.*, 2007, **19**, 1801.
25. A. Y. Khodakov, A. Griboval-Constant, R. Bechara and V. L. Zholobenko, *J. Catal.,* 2002, **206**, 230.
26. A. Hanif, T. Xiao, A. P. E. York, J. Sloan and M. L. H. Green, Chem. Mater., 2002, 14, 1009.
27. A. Cimino and B. A. De Angelis, *J. Catal.*, 1975, **36**, 11.
28. P. Delporte, F. d. r. Meunier, C. Pham-Huu, P. Vennegues, M. J. Ledoux and J. Guille, *Catal. Today*, 1995, **23**, 251.
29. P. Delporte, C. Pham-huu and M. J. Ledoux, *Appl. Catal. A*, 1997, **149**, 151.
30. T. Miyao, I. Shishikura, T. M. Matsuoka and M. Nagai, *Chem. Lett.*, 1996, **121**, 561.
31. T. Xiao, H. Wang, J. Da, K. S. Coleman and M. L. H. Green, *J. Catal.*, 2002, **211**, 183.
32. N. Wang, K. Fang, D. Jiang, D. Li and Y. Sun, *Catal. Today*, 2010, **158**, 241.
33. K. Fang, D. Li, M. Lin, M. Xiang, W. Wei and Y. Sun, *Catal. Today*, 2009, **147**, 133.
34. A. Muramatsu, T. Tatsumi and H. Tominaga, *J. Phys. Chem.*, 1992, **96**, 1334.